Eur. Phys. J. D (2019) 73: 236
https://doi.org/10.1140/epjd/e2019-100119-9

THE EUROPEAN PHYSICAL JOURNAL D

Regular Article

Attosecond pulse generation isolated with a polarization-ionization gating scheme

Wenqing Yu, Ning Su, Hao Song, and Gao Chen[a]

School of Science, Changchun University of Science and Technology, Changchun 130022, P.R. China

Received 4 March 2019 / Received in final form 12 August 2019
Published online 15 November 2019

Abstract. We theoretically simulate high harmonic generation in the frequency domain and attosecond pulse generation in the time domain from helium atom irradiated by a combined field, which is synthesized by a 4 fs, 800 nm x-polarized pulse and a 4 fs, 800 nm y-polarized pulse with a certain time delay. Different from harmonic spectrum generated by the x-polarized pulse alone, the harmonic spectrum from the combined field shows two supercontinuum regions, one supercontinuum spectrum with slight modulation ranges from the 35th to 90th order, and another supercontinuum spectrum ranges from the 185th to 285th order. This phenomenon is attributed to the dual gating of the harmonic emission by the polarization and the ionization in the case of combined pulses. After inverse Fourier transform, an isolated 108 as pulse can be obtained by superposing supercontinuum harmonics from the 185th to the 285th order.

1 Introduction

Ultrafast optics has developed rapidly in recent decades [1]. Among them, the generation of isolated attosecond (as) pulse has played an important and irreplaceable role in the study of phenomena in an extremely short time scale like electronic dynamics of atoms [2,3], molecules, and the nanostructures on metal surface [4]. Based on high order harmonic generation (HHG), isolated attosecond pulses have been realized in a few laboratories by few-cycle driving pulse scheme [5–7], ionization gating scheme [8], polarization gating scheme [9–11], attosecond lighthouse [12] and two-color pulse scheme [13]. So far, the shortest isolated attosecond pulse with 43 as pulse width was realized in the Wörner group by using the amplitude gating scheme [14].

Waveform-controlled light pulse has been playing a key role in the single isolated attosecond pulse generation. The use of the two-color laser field has shown great potential in generation of an arbitrary optical waveform. As originally proposed by Merdji and co-workers [15], the combination of a laser pulse with its spectrally detuned second harmonic restricts the HHG to a single half cycle of the driving pulse, so the generation of XUV continua with photon energies exceeding 150 eV has been achieved [16]. In this experiment two synchronized laser pulses at 1500 nm and 800 nm respectively were combined with parallel polarization. Zeng et al. obtained an isolated 65 as pulse by adopting a two color optical field synthesized by an intense 6 fs pulse at 800 nm and a relatively weak 21.3 fs pulse at 400 nm [17]. More recently, Takahashi et al. generated the isolated attosecond pulses with 500 as pulse duration and 1.3 μJ energy at approximately 30 eV [18]. For above two color field scheme, the underlying physics is that the laser field amplitude varies acutely between the two neighboring half-cycle, and the maximum electron return energy of each individual half-cycle is different. The broad XUV continuum spectrum that supports ultrashort attosecond pulse results from the enlarged difference of the cutoff energies between the highest and the second highest half-cycles. These studies on the two color field, however, are confined to the parallel polarized field, and one would wonder whether an isolated attosecond pulse can be achieved in an orthogonally polarized laser field. Xu obtained an isolated attosecond pulse with a duration of 16 as by adopting an orthogonally polarized laser field, which is synthesized by an 800 nm chirped laser pulse and an 800 nm chirp-free laser pulse [19]. Chang et al. obtained an isolated attosecond pulse with a 75 as duration by adding an electrostatic field in the y component to an orthogonally polarized two-color laser field, which is synthesized by a mid-infrared pulse (12.5 fs, 2000 nm) in the y component and a much weaker (12 fs, 800 nm) pulse in the x component [20]. Yu et al. demonstrated a single attosecond pulse generation by blocking the low order high harmonics on the attosecond pulse chain from an orthogonal two-color laser field consisting of a 9 fs, 800 nm pulse linearly polarized in the x direction and a 9 fs, 1300 nm pulse in the y direction [21].

It has been known for a long time that laser polarization is another important parameter for steering the electron motion. The polarization gating scheme, proposed

[a] e-mail: cgcust@hotmail.com

by Corkum et al. [22], relies on the fact that the emission intensity of high harmonic varies with the ellipticity of the driving laser pulse. When the ellipticity is 0.13, the conversion efficiency of high harmonics is only half that of linear polarization. By changing the polarization of the laser pulse from circular to linear and back to circular again, a short temporal gate can be formed for HHG emission. The scheme was first performed experimentally in 2006 by adjusting the delay between two counter-rotating circularly-polarized pulses to create a gate with a half cycle and nearly linearly polarized, and an isolated attosecond pulse with an energy of 70 pJ and a duration of 130 as was obtained by intercepting a supercontinuum of 25 eV–50 eV [23]. Practically, the unwanted ionization of the gas target caused by the laser cycles before the polarization gate places a limit on the pulse duration and intensity of the driving laser. The double optical gating technique adding a second harmonic field to polarization gating scheme relaxes the limit to some extent and has been used in the experiment of a 67 as isolated pulse generation [24].

In this work, we propose a new polarization gating scheme for obtaining isolated attosecond pulse by adopting an orthogonally polarized combined field consisting of a 4 fs, 800 nm pulse linearly polarized in x component and a 4 fs, 800 nm pulse linearly polarized in y component. When the time delay between two pulses is properly adjusted, the polarization of the laser pulse changes from linear to elliptical and back to linear again, different from usual polarization gating pulse whose polarization changes from circular to linear and back to circular again. This technique can be realized in the following way. When Ti: sapphire pulse passes through a quartz crystal, it becomes two pulses with different propagation speed, orthogonal polarization direction, and the same or different amplitudes. By appropriately adjusting the angle between the optical axis of the quartz crystal and the direction of polarization of the incident pulse and the thickness of the quartz crystal, two output pulses with same amplitude and a certain time delay can be obtained. Thus the synthesized electric field exhibits linear polarization characteristics in the leading and trailing parts of pulse, and elliptical polarization in the middle. Since elliptically polarized field does not make a major contribution to high harmonics, harmonic mainly come from linearly polarized field at the leading and trailing parts of pulse. Here, in order to avoid interference between the harmonics from the leading and the trailing electric fields, we control the amplitude of the electric field to deplete the electrons in the atom before the end of the elliptic polarized field. Thus, an isolated attosecond pulse can be obtained because only the linear polarized field at the leading part contributes to high harmonics. Obviously, this scheme is very similar to the ionization gating scheme in which the electrons in the ground state are completely ionized by the leading of the electric field by increasing the electric field intensity [25], so we term this new scheme as polarization-ionization gating scheme.

Compared with ionization gating and polarization gating schemes, polarization-ionization gating scheme has the following advantages. The success of the ionization gating depends on the rapid ionization of electrons caused by strong electric field, however such rapid ionization will result in phase mismatch in the process of high harmonic propagation. In polarization-ionization gating scheme, we can give similar harmonic emission process with low electric field but overcome the phase mismatch condition in the process of the harmonic propagation. In the polarization gating scheme, harmonic emission occurs in the polarization gate that a half-cycle region in which the total field ellipticity is below the threshold ellipticity. Since no other optical cycles contribute to the generation of high harmonics, the laser cycles on the leading of the pulse cause unwanted ionization of the gas target before the arrival of the linear cycle. This results in a decrease in the distribution of the ground state electrons and further a decrease in the ionization probability in the linear polarization region. However, in the polarization-ionization gating scheme, there is no loss of ground state electrons before the linear polarized electric field.

2 Theoretical methods

Lewenstein's strong-field approximation model [26–28] have been used in our calculation to simulate the harmonic spectra from a single atom submitted to the polarization-ionization gating pulse. Since the ellipticity of the laser pulse changes over time, the dipole moments in two different directions need to be calculated separately. If we set the early arrival pulse to be linearly polarized along the x direction and the post-arrival pulse to be linearly polarized along the y direction, then only harmonic spectrum along the x direction needs to be considered because the amplitude of the electric field is controlled to deplete the electrons in the atom before the end of the elliptic polarized field. So the electric field polarized in the y direction has no chance to produce high harmonics. The electronic time-dependent dipole moment in the external field can be described as [29] (unless otherwise stated, atomic units are used throughout this paper)

$$\begin{aligned} d_{nl}(t) \approx i \int_{-\infty}^{t} dt' \left(\frac{\pi}{\varepsilon + i(t-t')/2}\right)^{3/2} d_x^* \left[\vec{p}_{st}\left(t',t\right) - \vec{A}(t)\right] \\ \times \exp[-iS_{st}(\vec{p}_{st},t',t)]\vec{d}\left[\vec{p}_{st}(t',t) - \vec{A}(t')\right] \cdot \vec{E}(t') \\ \times \exp\left[-\int_{-\infty}^{t} \omega(t''d\ t'')\right] + c.c. \end{aligned} \tag{1}$$

Where ε is a small positive number, $\vec{A}(t)$ is the vector potential of electric field $\vec{E}(t)$, and the two-dimensional combined electric field $\vec{E}(t)$ is given by

$$\begin{aligned} \vec{E}(t) = \vec{x}E_x f_x(t)\cos(\omega_x t + \phi_{\mathrm{CEP}} + \phi_{td}) \\ + \vec{y}E_y f_y(t)\cos(\omega_y t + \phi_{\mathrm{CEP}}). \end{aligned} \tag{2}$$

E_x and E_y are the peak amplitudes of electric field. ω_x and ω_y are the frequencies in the x and y directions, respectively. The initial phase ϕ_{CEP} is set as 0.7π and the carrier envelopes in the x and y directions are as follows,

$$f_x\left(t\right) = \exp[-2\ln 2\left(t + td/2\right)^2/\tau_x^2] \tag{3}$$

$$f_y(t) = \exp[-2\ln 2\,(t - td/2)^2/\tau_y^2]. \quad (4)$$

Here τ_x and τ_y are the pulse durations (full width at half maximum) and td is the time difference between the peaks of two electric fields. The phase difference $\phi_{td} = td \times \omega_x$ is introduced due to the time difference between the two pulses.

In equation (1), the stationary momentum $\vec{p}_{st}$ and the quasiclassical action S_{st} are given by

$$\vec{p}_{st}(t', t) = \frac{1}{t - t'} \int_{t'}^{t} \vec{A}(t'')t'', \quad (5)$$

$$S_{st}(\vec{p}_{st}, t', t) = (t - t')I_P - \frac{1}{2}p_{st}^2(t', t)(t - t') + \frac{1}{2}\int_{t'}^{t} A^2(t'')t''. \quad (6)$$

Here I_P is the ionization potential of the helium atom. The approximation of electric dipole $\vec{d}(\vec{p})$ for hydrogen-like atoms is

$$\vec{d}(\vec{p}) = i\frac{2^{7/2}(2I_P)^{5/4}}{\pi}\frac{\vec{p}}{(p^2 + 2I_P)^3}. \quad (7)$$

According to the Ammosov, Delone, Krainov (ADK) model [30], the ionization rate in equation (1) can be calculated as

$$\omega(t) = \omega_P |C_{n^*}|^2 \left(\frac{4\omega_P}{\omega_t}\right)^{2n^*-1} \exp\left(-\frac{4\omega_P}{3\omega_t}\right), \quad (8)$$

where $\omega_P = I_P$, $n^* = Z\left(\frac{I_{ph}}{I_P}\right)^{1/2}$, $\omega_t = \frac{|E(t)|}{\sqrt{2I_P}}$ and $|C_{n^*}|^2 = \frac{2^{2n^*}}{n^*\Gamma(n^*+1)\Gamma(n^*)}$, in which Z is the net resulting charge of the helium atom, and I_{ph} is the ionization potential of the hydrogen atom.

We can calculate dipole acceleration from the time-dependent dipole moment $a(t) = \frac{d^2}{dt^2}d_{nl}(t)$. The harmonic spectrum is then obtained by Fourier transforming the time-dependent dipole acceleration:

$$P_A(\omega) = \left|\frac{1}{t_f - t_i}\frac{1}{\omega^2}\int_{t_i}^{t_f} a(t)\,e^{-i\omega t}dt\right|^2. \quad (9)$$

An ultrashort attosecond pulse can be generated by superposing several harmonics on the harmonic spectrum

$$I(t) = \left|\sum_q a_q e^{iq\omega t}\right|^2, \quad (10)$$

where $a_q = \int a(t)e^{-iq\omega t}dt$.

3 Results and discussion

As mentioned above, we can obtain two linearly polarized pulses with orthogonal polarization direction, equal amplitude and a certain time delay when a linearly polarized Ti: sapphire pulse passes through a suitable quartz crystal. Here time delay between two pulse peaks is set as 1.25 times optical period by adjusting the thickness of the quartz crystal and the two pulses have the same amplitudes ($E_x = E_y = 0.28$ a.u.) by changing the angle between the incident pulse polarization and the optical axis of the quartz crystal. Both the pulse laser parameters and the atomic parameters can be adjusted. The reason for choosing a high pulse intensity is to control the atomic ionization probability and drastically extend the cutoff position of the harmonic spectrum. Even if the pulse laser intensity is appropriately lowered, the scheme is still effective. The duration of the input pulses is 4 fs. In Figure 1, we in turn show variations of the electric fields of two pulses and the total electric field with time. The green and the black curves show the amplitude evolution of the x-polarized and y-polarized fields with time, respectively, and the synthesized electric field is shown by a red curve in Figure 1. It can be clearly seen from the figure that the leading of the electric field is linearly polarized pulse in x direction, the trailing of the electric field is linearly polarized pulse in y direction, and the middle part is an elliptically polarized pulse whose ellipticity changes with time.

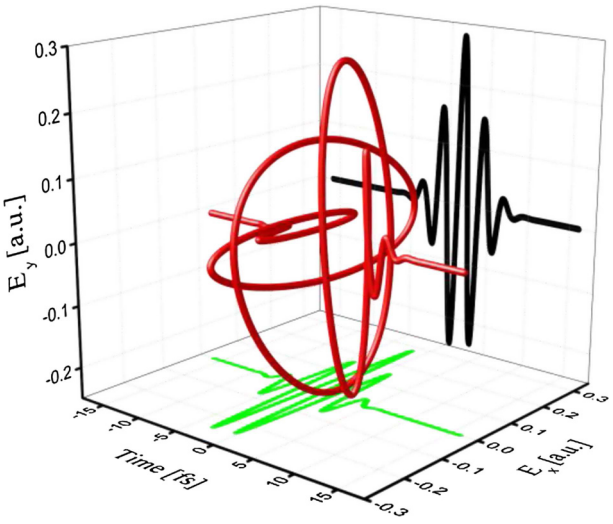

Fig. 1. x-polarized field with peak amplitude $E_x = 0.28$ a.u. (green), y-polarized field with peak amplitude $E_y = 0.28$ a.u. (black) and the total field (red) are plotted as a function of time.

To understand the physics behind polarization-ionization gating scheme, we firstly simulate the HHG spectra. Figure 2b gives the HHG spectrum from a single helium atom subjected to this new polarization pulse. For comparison, we also show the HHG spectrum from the same helium atom subjected to the x-polarized pulse alone, as shown in Figure 2a. It can be seen from Figures 2a and 2b that the cut-off positions of the harmonic spectra in the two cases are obviously different. When the x-polarized pulse alone is used as the driving pulse, the cut-off position of the high harmonic spectrum is 345th order, and the supercontinuum is covered with the spectral range from 290th to 345th order. When the synthesized pulse is used as the driving pulse, the cut-off position of the harmonic spectrum is shortened to 285th order and the supercontinuum of the harmonic spectrum

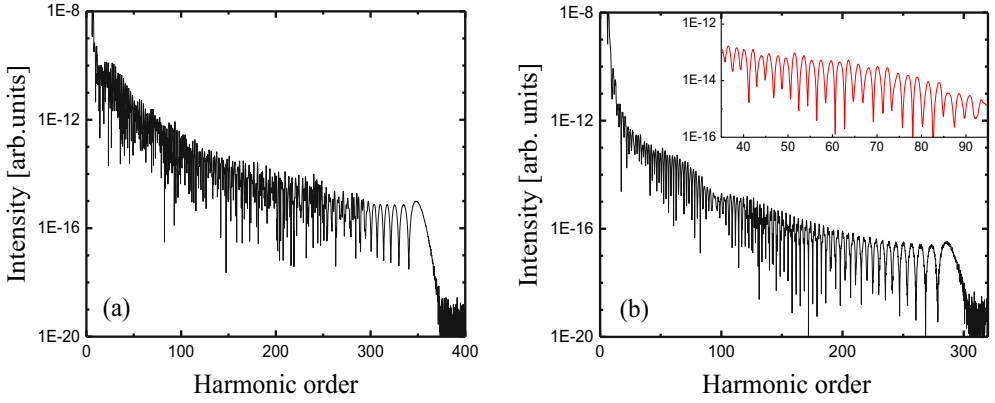

Fig. 2. (a) HHG spectrum from helium atom exposed to an 800 nm fundamental pulse with a peak amplitude $E_x = 0.28$. (b) HHG spectrum from helium atom exposed to the synthesized pulse. For a clear look of the harmonic order, we offer the amplification of HHG spectra from 35th to 95th in the inset.

appears in two regions. The first supercontinuum with slight modulation is covered with the spectral range from the 35th to 90th order and the second supercontinuum is covered with the spectral range from the 185h to 285th order. Obviously, the bandwidth of the supercontinuum spectrum is greatly extended in the case of the synthesized pulse.

In the following, a semi-classical three-step model theory [31] is used to analyze the dynamical behavior of electrons in the case of the synthesized field, further explain above supercontinuum broadening. The physical origin of HHG can be described by the semiclassical three-step model involving ionization, acceleration and recombination. Specifically, the electron first tunnels through the effective potential barrier formed by the atom and the laser field, then oscillates in the field, and, finally, may recombine with the parent ion and emit a harmonic photon with an energy equal to the ionization potential plus the kinetic energy of the recombining electron. Obviously, the electron ionized at different time in the laser field has a certain moment of recombination with the parent ion and a certain kinetic energy at this recombination moment. In Figures 3a and 3c, the black thick and thin solid curves show the evolution of the x-polarized and y-polarized electric fields with time, respectively, and the filled red region denotes the corresponding ionization rate, which comes from the derivative of the ionization probability (calculated from the ADK model) versus time. The area of the filled region is physically defined as the relative ionization amount of electrons. According to the three-step model theory, the kinetic energies of the electron recombined with the parent ions as a function of ionization (black dot curve) and recombination time (blue dot curve) are shown in Figures 3b and 3d Here, we have converted the kinetic energy of the electron into the orders of the harmonics.

It can be seen from Figure 3a that in the x-polarized field case alone, there exists ionization peaks at moments A, B, C, D and E. And in Figure 3b, when the electrons ionized at these ionization peaks recombine with parent ions, the maximum order of harmonic radiation are in turn 133rd, 290th, 345th, 243rd and 100th. The interference between these harmonics results in the strong modulation of the spectrum, further cause to the shorter supercontimuum range. On the contrary, in the case of the synthesized field in Figure 3c, the trajectories of the electrons ionized at the same moments of x-polarized field are changed due to the superimposing of y-polarized field. In Figure 3d, we only can see the trajectories of the electrons ionized around moment A and B. When the electron is ionized at moment A, the maximum order of the harmonic radiation is 110th. Similarly when the electron is ionized at moment B, the maximum order of the harmonic radiation is 285th. While the electrons ionized at moment C, D, E, F, G and H will be drove away from the parent ion by joint force of x-polarized field and y-polarized field, and can't recombine with parent ion, so Figure 3d does not give the recombination information of these electrons. We obtain the conclusion that the cut-off position of the harmonic spectrum is shortened and the bandwidth of the supercontinuum spectrum is greatly extended in Figure 2b.

From the above analysis, it can be found that although the cut-off positions obtained from quantum mechanical calculation is nearly the same as the result obtained from semi-classical three-step model in the case of the synthesized field, the range of supercontinuum bandwidth is significantly different. According to semi-classical calculation shown in Figure 3d, the super-continuum spectrum should be covered with spectral range from 110th to 285th order, and the harmonics before 110th order experience weak modulation because of weak ionization at moment A. Actually, the supercontinuums of the harmonic spectrum in Figure 2b occur in two spectral regions of 35th to 90th order and 185th to 285th order. In the following, we will explain this inconsistency in detail by means of the time-frequency analysis.

Figure 4 shows the time-frequency analysis of the harmonics from helium atom subjected to the combined pulse. It can be seen that for the harmonics ranging from 185th to 285th order, only the peak P_2 makes contribution to HHG, and there are two branches at the left and right sides of the peak P_2, where the left branch corresponds to the short trajectory and the right one corresponds to the long trajectory. It also can be seen that the left

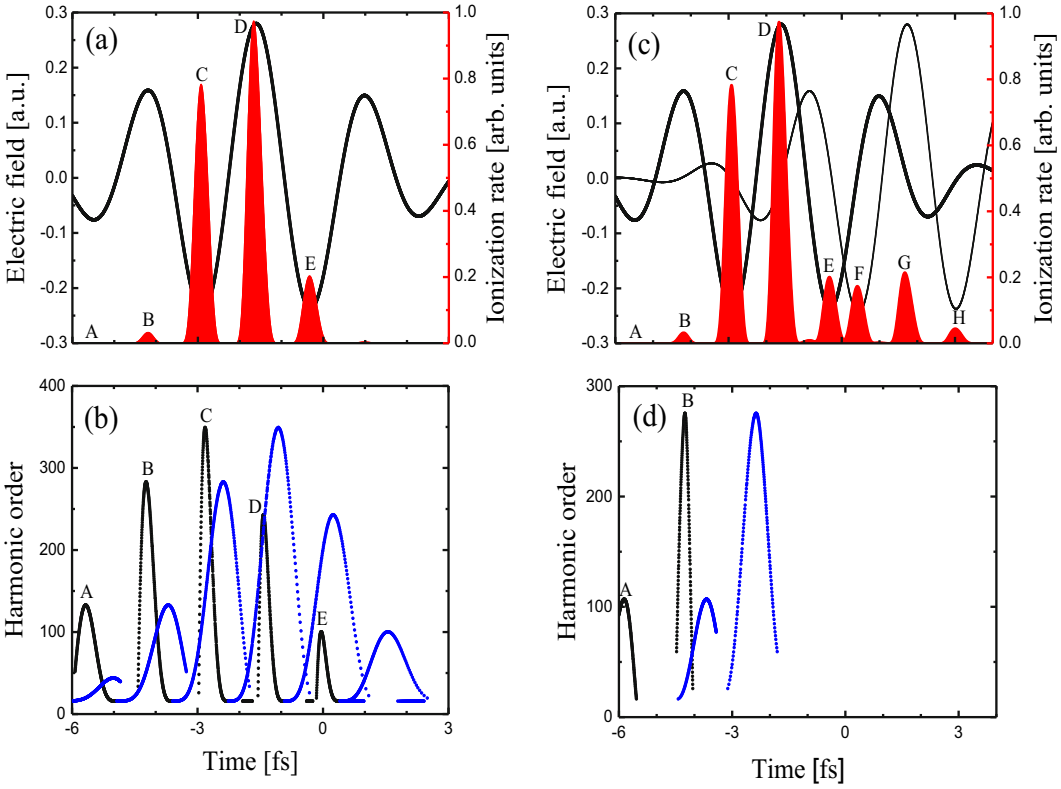

Fig. 3. (a) In the case of the x-polarized pulse alone, the x-polarized field with peak amplitude 0.28 (black thick line) and the ionization rate of the helium atom (filled red region) as a function of time. (c) In the case of the synthesized pulses, the x-polarized field (black thick line), the y-polarized field (black thin line) and the ionization rate of the helium atom (filled red region) as a function of time. Electron trajectories of HHG (the ionization and recombination times are shown in black and blue dot curves, respectively): (b) in the case of the x-polarized pulse alone; (d) in the case of the synthesized pulses.

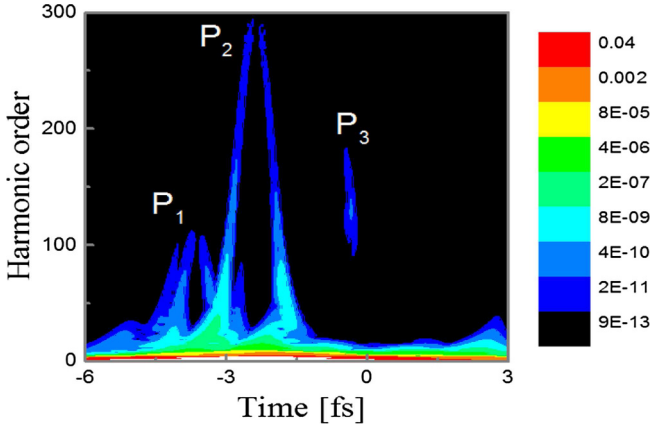

Fig. 4. Time-frequency analysis of the harmonics generated from helium atom irradiated by the combined field.

branch is equal to the right one in intensity, indicating that the short trajectory and the long trajectory make equal contribution to harmonic generation. This conclusion is consistent with the second supercontinuum range of the harmonic spectrum given in Figure 2b. As for the harmonics before 110th order, both P_1 and P_2 make contribution to HHG, but the intensity of P_2 is clearly stronger than that of P_1, so the harmonics before 110th order experience weak modulation. Here it needs to be pointed out that in Figure 4, in addition to P_1 and P_2, there appears a P_3 which mainly contributes to 90th to 185th order harmonics, and intensity of P_3 is very close to P_2. The appearance of P_3 explains the disappearance of the supercontinuum spectrum in this range in Figure 2b.

Obviously, the characteristics of the harmonic spectrum obtained from quantum mechanical calculation are consistent with those obtained by the time-frequency analysis in the case of the synthesized field. However, in the calculation of the electron trajectory in Figure 3d, the harmonic radiation from P_3 branch does not appear. This is because in the classical calculation of the three-step model, only the electrons that return exactly to the parent ion contribute to the harmonic emission. However, in the quantum calculation of the high harmonic generation, even if the ionized electrons return to a distance a little further from the parent ion, it still contributes to the harmonic generation. The intensity of the harmonic depends on the closest distance of the ionized electrons to the parent ion and the ionization rate of the electrons at the time of ionization. In Figure 5, we show the ionization rate (filled red region), ionization probability (black solid) of the helium atom, and the closest distances of ionized electrons to the parent ion (blue solid). It can be seen that the closest distances of electrons to the parent ion are different when electrons are ionized around moment A, B, C, D, E, F, G and H, respectively. Specifically, the closest distance

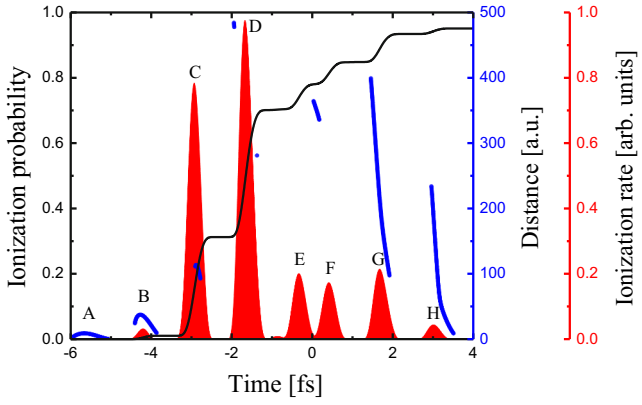

Fig. 5. In the case of combined pulses, the ionization rate (filled red region), ionization probability (black) of helium atom and the closest distance of electron to nucleus as a function of time (blue).

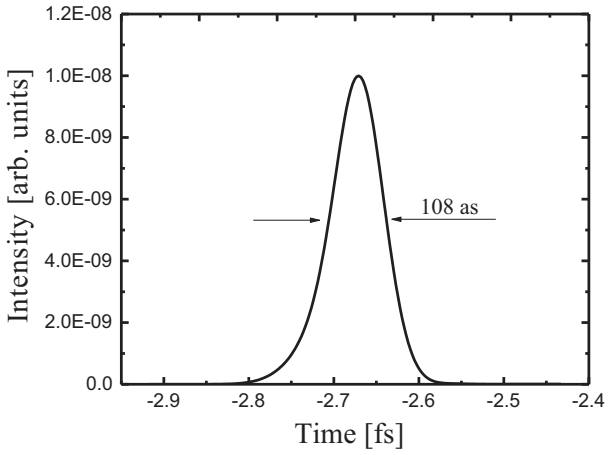

Fig. 6. Isolated attosecond pulse obtained by superposing the harmonics from the 185th order to the 285th order.

of electrons to the parent ion is 1–9 a.u. when electrons are ionized around moment A, and the closest distance of electrons to the nucleus is 10–37 a.u. when electrons are ionized around moment B. Correspondingly, the closest distances are almost more than 100 a.u. when the electrons are ionized around moment D, E, F and G, respectively. Obviously, the electrons ionized around moment D, E, F, and G cannot go back to the parent ion vicinity because of the driving of y-polarized field, so they cannot contribute to high harmonics generation. On the contrary, the electrons ionized around moment A and B can go back to the vicinity of nuclear and contribute to high harmonics generation. As for the case of electrons ionized around moment H, a small portion of electrons can return very near to nucleus, however the harmonic emission still can't be accomplished due to the severe depletion of electrons within helium atom (ionization probability of atom has reached 95% at moment H). Here the key focus is whether the electrons ionized around moment C contribute to harmonic generation. We need to consider the closest distance of the electrons to the parent ion and the ionization rate of the electrons at the time of ionization. Although the electrons can be driven back to the nearest position of 93–113 a.u. from the parent ion, which is much further than the closest distance of the electron ionized around moment A and B, the atomic ionization rate (0.8) is much higher than those at moment A (8×10^{-7}) and B (0.032). So these electrons also will have a small contribution to high order harmonic generation. This result is in good agreement with three harmonic emission peaks given by time-frequency analysis in Figure 4.

In addition, since the ionization rate around time A is much lower than that around time B, it contributes less to the high harmonic emission than those ionized around moment B. This leads to the weak interference between the harmonics before 110th order and further a weak modulation on the first supercontinuum spectrum on Figure 2b. By the above analysis, we give the reason for the appearance of the two parts of supercontinuum on high harmonic spectrum in Figure 2b.

Finally, by inverse Fourier transform, we give the attosecond pulse generation in the time domain from the polarization-ionization gating scheme. As shown in Figure 6, an isolated attosecond pulse with a duration of 108 as can be obtained by superposing harmonics from 185th to 285th order.

4 Conclusion

In this paper, we numerically investigate the HHG spectra generated from helium atom irradiated by a combined field consisting of a 4 fs, 800 nm x-polarized pulse and a 4 fs, 800 nm y-polarized pulse. It is found that there are two supercontinuum regions on the harmonic spectrum, one supercontinuum spectrum with slight modulation ranges from 35th to 90th order, and another supercontinuum spectrum ranges from 185h to 285th order. By the calculation of the semi-classical three-step model, the time-frequency analysis of harmonics and the closest distance of electrons to the parent ion, we give detailed explanation of the supercontinuum harmonic generation. Finally, an isolated attosecond pulse with a duration of 108 as is obtained by superposing harmonic from 185th to 285th order. In the following work, we will further explore the study on extending the supercontinuum bandwidth by considering the phase mismatch of P_3 harmonics in the process of propagation in macroscopic media.

This work was supported by the Jilin Provincial Research Foundation for Basic Research, China (Grants No. 20170101046JC). Any opinions, findings and conclusions or recommendations expressed in this material are those of the authors and do not necessarily reflect the views of the Jilin Provincial Research Foundation.

Author contribution statement

All authors contributed equally to the paper.

References

1. F. Krausz, M. Ivanov, Rev. Mod. Phys. **81**, 163 (2009)

2. R. Kienberger, E. Goulielmakis, M. Uiberacker, A. Baltuska, V. Yakovlev, F. Bammer, A. Scrinzi, Th. Westerwalbesloh, U. Kleineberg, U. Heinzmann, M. Drescher, F. Krausz, Nature **427**, 817 (2004)
3. J.G. Chen, Y.J. Yang, J. Chen, B.B. Wang, Phys. Rev. A **91**, 043403 (2015)
4. M.I. Stockman, M.F. Kling, U. Kleineberg, F. Krausz, Nat. Photonics **1**, 539 (2007)
5. E. Goulielmakis, M. Schultze, M. Hofstetter, V.S. Yakovlev, J. Gagnon, M. Uiberacker, A.L. Aquila, E.M. Gullikson, D.T. Attwood, R. Kienberger, F. Krausz, U. Kleineberg, Science **320**, 1614 (2008)
6. F. Ferrari, F. Calegari, M. Lucchini, C. Vozzi, S. Stagira, G. Sansone, M. Nisoli, Nat. Photonics **4**, 875 (2010)
7. G. Sansone, E. Benedetti, F. Calegari, C. Vozzi, L. Avaldi, R. Flammini, L. Poletto, P. Villoresi, C. Altucci, R. Velotta, S. Stagira, S. De Silvestri, M. Nisoli, Science **314**, 443 (2006)
8. W. Cao, P. Lu, P. Lan, X. Wang, G. Yang, Phys. Rev. A **74**, 063821 (2006)
9. P. Tzallas, E. Skantzakis, C. Kalpouzos, E.P. Benis, G.D. Tsakiris, D. Charalambidis, Nat. Phys. **3**, 846 (2007)
10. S. Gilbertson, S.D. Khan, Y. Wu, M. Chini, Z. Chang, Phys. Rev. Lett. **105**, 093902 (2010)
11. X. Feng, S. Gilbertson, H. Mashiko, H. Wang, S.D. Khan, M. Chini, Y. Wu, K. Zhao, Z. Chang, Phys. Rev. Lett. **103**, 183901 (2009)
12. H. Vincenti, F. Quéré, Phys. Rev. Lett. **108**, 113904 (2012)
13. E.J. Takahashi, P. Lan, O.D. Mücke, Y. Nabekawa, K. Midorikawa, Phys. Rev. Lett. **104**, 233901 (2010)
14. T. Gaumnitz, A. Jain, Y. Pertot, M. Huppert, I. Jordan, F. Ardana-Lamas, H.J. Wörner, Opt. Express. **25**, 27506 (2017)
15. H. Merdji, T. Auguste, W. Boutu, J-P. Caumes, B. Carré, T. Pfeifer, A. Jullien, D.M. Neumark, S.R. Leone, Opt. Lett. **32**, 3134 (2007)
16. C. Vozzi, F. Calegari, F. Frassetto, L. Poletto, G. Sansone, P. Villoresi, M. Nisoli, S. De. Silvestri, S. Stagira, Phys. Rev. A **79**, 033842 (2009)
17. Z. Zeng, Y. Cheng, X. Song, R. Li, Z. Xu, Phys. Rev. Lett. **98**, 203901 (2007)
18. E.J. Takahashi, P. Lan, O. D. Mücke, Y. Nabekawa, K. Midorikawa, Nat. Commun. **4,** 2691 (2013)
19. J. Xu, Phys. Rev. A **83**, 033823 (2011)
20. L.X. Chang, G.T. Zhang, J. Wu, X.S. Liu, Phys. Rev. A **81**, 043420 (2010)
21. Y. Yu, X. Song, Y. Fu, R. Li, Y. Cheng, Z. Xu, Opt. Lett. **16**, 686 (2008)
22. P.B. Corkum, N.H. Burnett, M.Y. Ivanov, Opt. Lett. **19**, 1870 (1994)
23. I.J. Sola, E. Mevel, L. Elouga, E. Constant, V. Strelkov, L. Poletto, P. Villoresi, E. Benedetti, J.P. Caumes, S. Stagira, C. Vozzi, G. Sansone, M. Nisoli, Nat. Phys. **2**, 319 (2006)
24. K. Zhao, Q. Zhang, M. Chini, Y. Wu, X.W. Wang, Z.H. Chang, Opt. Lett. **37**, 3891 (2012)
25. M.J. Abel, T. Pfeifer, P.M. Nagel, W. Boutu, M.J. Bell, C. P. Steiner, D.M. Neumark, S.R. Leone, Chem. Phys. **366**, 9 (2009)
26. L.V. Keldysh, Zh. Eksp. Teor. Fiz. **47**, 1945 (1964)
27. F.H.M. Faisal, J. Phys. B **6**, L89 (1973)
28. H.R. Reiss, Phys. Rev. A **22**, 1786 (1980)
29. M. Lewenstein, P. Salieres, A. L'Huillier, Phys. Rev. A **52**, 4747 (1995)
30. M.V. Ammosov, N.B. Delone, V. Krainov, Zh. Eksp. Teor. Fiz. **91**, 2008 (1986)
31. P.B. Corkum, Phys. Rev. Lett. **71**, 1994 (1993)